Signal Processing 93 (2013) 1976–1987

Contents lists available at SciVerse ScienceDirect

Signal Processing

journal homepage: www.elsevier.com/locate/sigpro

Subspace techniques for multidimensional model order selection in colored noise ☆

Kefei Liu [a,*], João Paulo C.L. da Costa [b], Hing Cheung So [a], Lei Huang [c]

[a] Department of Electronic Engineering, City University of Hong Kong, Kowloon, Hong Kong, China
[b] Department of Electrical Engineering, University of Brasília, Brasília, Brazil
[c] Department of Electronic and Information Engineering, Harbin Institute of Technology Shenzhen Graduate School, Shenzhen, China

ARTICLE INFO

Article history:
Received 12 September 2012
Received in revised form
7 January 2013
Accepted 29 January 2013
Available online 8 February 2013

Keywords:
Model order selection
Estimation error
Colored noise
Shift invariance
Multidimensional harmonic retrieval
Multilinear algebra

ABSTRACT

R-dimensional (R-D) harmonic retrieval (HR) in colored noise, where $R \geq 2$, is required in numerous applications including radar, sonar, mobile communications, multiple-input multiple-output channel estimation and nuclear magnetic resonance spectroscopy. Tensor-based subspace approaches to R-D HR such as R-D unitary ESPRIT and R-D MUSIC provide super-resolution performance. However, they require the prior knowledge of the number of signals. The matrix based (1-D) ESTimation ERror (ESTER) is subspace based detection method that is robust against colored noise. To estimate the number of signals from R-D measurements corrupted by colored noise, we propose two R-D extensions of the 1-D ESTER by means of the higher-order singular value decomposition. The first R-D ESTER combines R shift invariance equations each applied in one dimension. It inherits and enhances the robustness of the 1-D ESTER against colored noise, and outperforms the state-of-the-art R-D order selection rules particularly in strongly correlated colored noise environment. The second R-D scheme is developed based on the tensor shift invariance equation. It performs best over a wide range of low-to-moderate noise correlation levels, but poorly for high noise correlation levels showing a weakened robustness to colored noise. Compared with the existing R-D ESTER scheme, both proposals are able to identify much more signals when the spatial dimension lengths are distinct.

1. Introduction

Multidimensional harmonic retrieval (HR) [1] has numerous applications such as multiple-input multiple-output (MIMO) radar imaging [2], channel estimation in wireless communication systems [3–5], nuclear magnetic resonance (NMR) spectroscopy [6,7], source localization and tracking [8–12]. For example, the measurements in NMR spectroscopy, which is a powerful technique for protein research in food and nutritional industries, can be modeled as a sum of multidimensional damped sinusoids where the frequencies and damping factors are crucial to determining the protein structures. In MIMO radar system, the sinusoidal parameters of the MIMO radar data contain the position information of multiple targets of interest such as direction-of-arrival (DoA), direction-of-departure (DoD), time-of-arrival (ToA), and Doppler frequency. Moreover, in wireless communications, the extracted physical parameters from multidimensional channel sounding measurements contain the information about the channel characteristics such as the scatterer distribution, dominant propagation paths, and coherence time. They can then be exploited to adjust the channel model parameters, or to optimize the wireless network layout to guarantee high channel capacity.

☆ The work described in this paper was supported by a grant from the NSFC/RGC Joint Research Scheme sponsored by the Research Grants Council of the Hong Kong and the National Natural Science Foundation of China (Project No.: N_CityU 104/11, 61110229).

* Corresponding author. Tel.: +852 3442 2021; fax: +852 3442 0562.
E-mail addresses: kefeilau@gmail.com (K. Liu), jpdacosta@unb.br (J.P.C.L. da Costa), hcso@ee.cityu.edu.hk (H. Cheung So), lhuang@hitsz.edu.cn (L. Huang).

0165-1684/$ - see front matter © 2013 Elsevier B.V. All rights reserved.
http://dx.doi.org/10.1016/j.sigpro.2013.01.022

Tensor-based subspace approaches to R-dimensional (R-D) HR, where $R \geq 2$, include 2-D unitary ESPRIT [13], R-D unitary ESPRIT and its variants [14–16], R-D MUSIC [17], multidimensional folding (MDF) [12], improved MDF [18], R-D rank reduction estimator (RARE) [19] and principal-singular-vector utilization for modal analysis (PUMA) [20,21]. By taking into account the multidimensional structure, these methods provide super-resolution estimation performance. However, they rely on the *a priori* knowledge of the number of signals, which is often unknown and must be estimated from the noisy multidimensional measurements. As a result, estimating the signal number from the data is an important issue. It is expected that reliable source enumeration is crucial to achieving accurate parameter estimates.

For detection of the number of signals from noisy R-D measurements, R-D order selection rules [22,23] should be applied. In these R-D rules, the measurement tensor is unfolded along the temporal dimension or other dimensions, and the conventional matrix-based (1-D) order selection rule such as minimum description length (MDL) [24], Akaike information criterion (AIC) [25], exponential fitting test (EFT) [26] or random matrix theory (RMT) algorithm [27,28] is applied in the resultant matrix for signal number detection. By combining the information of several unfolded matrices, the R-D rules provide an improvement in probability of correct detection (PoD). However, like their 1-D counterparts, these methods rely on the additive white noise assumption. In the presence of colored noise, which is commonly encountered in HR applications [29–32], they tend to overestimate the number of signals.

In [33], the matrix based estimation error (ESTER) has been proposed for source enumeration from a noisy mixture of exponentially damped or undamped complex sinusoids (uniform 1-D HR model). By utilizing the shift invariance property of the signal subspace spanned by the sinusoids, the ESTER is more robust against colored noise than traditional eigenvalue based order selection rules. Later in [34], an improved version of ESTER called subspace-based automatic model order selection (SAMOS) is developed by exploiting the singular values of the signal subspace matrix. Although with better performance, the number of identifiable signals of SAMOS is reduced by half compared with ESTER.

To apply the ESTER for estimating the number of signals in noisy R-D sinusoids model (uniform R-D HR model), an R-D extension of the matrix-based ESTER is proposed [35] by utilizing the higher-order singular value decomposition (HOSVD) of the measurement tensor. However, it is based on an empirical combination of the shift invariance equalities in individual dimensions. As a result, its performance is degraded in several scenarios. Moreover, the number of identifiable signals is limited to the minimum spatial dimension length minus 2.

In this work, we propose two multidimensional extensions of the matrix-based ESTER scheme by means of the HOSVD. The first proposal is based on the combination of R shift invariance equations each applied in a matrix unfolding. It directly extends the matrix-based ESTER [33] in a sense that the cost function in the criterion is the product of that of 1-D ESTER applied in each mode and is directly related to the variance of the biased multidimensional frequency estimates. By combining R sets of singular vectors of the HOSVD of the measurement tensor, it has strengthened robustness against colored noise, and remarkably outperforms the 1-D ESTER applied in each matrix unfolding as well as the existing R-D ESTER [35] in strongly correlated colored noise environment. For low-to-moderate noise correlation levels, the performance improvement is marginal. To further improve the performance for low-to-moderate noise correlation levels, the second proposal is developed based on the tensor shift invariance equation. By including the core tensor of the HOSVD in the subspace tensor used in the tensor shift invariance equation, it results in more reliable performance than the existing R-D ESTER scheme and has the best performance for weakly or moderately correlated colored noise. The identifiability of both proposed extensions is increased to the maximum spatial dimension length minus 2, which is a significant improvement over [35] when the spatial dimension lengths are distinct from each other.

The remainder of this paper is organized as follows. After reviewing the matrix and tensor notation in Section 2, the R-D HR data model is presented in Section 3. The matrix-based ESTER scheme for MOS is reviewed in Section 4. Then two R-D extensions of the matrix-based ESTER are developed in Section 5. Simulation results in Section 6 confirm the improved performance of the proposed R-D approaches. In Section 7, conclusions are drawn.

2. Matrix and tensor notation

In order to facilitate the distinction between scalars, matrices and tensors, the following notation is used: Scalars are denoted as italic letters (a, b, …, A, B, …, α, β, …), column vectors as lower-case bold-face letters ($\boldsymbol{a}$, $\boldsymbol{b}$, …), matrices as bold-face capitals ($\boldsymbol{A}$,$\boldsymbol{B}$,…), and tensors as bold-face calligraphic letters ($\boldsymbol{\mathcal{A}}$, $\boldsymbol{\mathcal{B}}$, …). Lower-order parts are consistently named: the (i,j)-entry of a matrix $\boldsymbol{A}$ is denoted as $a_{i,j}$, and the (i,j,k)-entry of a third-order tensor $\boldsymbol{\mathcal{X}}$ as $x_{i,j,k}$. The superscripts T and † stand for matrix transposition and the Moore–Penrose pseudo inverse, respectively. The $\|\boldsymbol{A}\|_2$ denotes the spectral norm of $\boldsymbol{A}$, and $\|\cdot\|_F$ denotes the Frobenius norm of a matrix or tensor, which is defined as the square root of the sum of squared magnitudes of all its elements.

The tensor operations are aligned with [36]: The r-mode vectors of a tensor $\boldsymbol{\mathcal{T}} \in \mathbb{C}^{I_1 \times I_2 \times \cdots \times I_R}$ are obtained by varying the r-th index within its range $(1,\ldots,I_r)$ and keeping all other indices fixed. The r-mode unfolding of $\boldsymbol{\mathcal{T}}$, symbolized by $[\boldsymbol{\mathcal{T}}]_{(r)} \in \mathbb{C}^{I_r \times (I_1 I_2 \cdots I_{r-1} I_{r+1} \cdots I_R)}$, is a matrix that collects all the r-mode vectors of $\boldsymbol{\mathcal{T}}$. The order of the columns is chosen in accordance with [36]. The r-mode product of $\boldsymbol{\mathcal{T}}$ and $\boldsymbol{U} \in \mathbb{C}^{J_r \times I_r}$ along the r-th mode is denoted as $\boldsymbol{\mathcal{T}} \times_r \boldsymbol{U} \in \mathbb{C}^{I_1 \times I_2 \cdots \times J_r \cdots \times I_R}$. It is obtained by multiplying the r-mode unfolding of $\boldsymbol{\mathcal{T}}$ from the left-hand side by $\boldsymbol{U}$.

3. Data model

For the pure uniform multidimensional HR problem [1], the noisy observations are modeled as a superposition of d

undamped or damped R-D complex sinusoids (cisoids):

$$x_{m_1,m_2,\ldots,m_R,n} = \sum_{i=1}^{d} s_i(n) \prod_{r=1}^{R} e^{(m_r-1)\cdot(\zeta_i^{(r)}+j\cdot\mu_i^{(r)})} + n^{(c)}_{m_1,m_2,\ldots,m_R,n},$$

$$m_r = 1,\ldots,M_r,\ r = 1,\ldots,R; \quad n = 1,\ldots,N, \tag{1}$$

where $\mu_i^{(r)}$ and $\zeta_i^{(r)} \le 0$ represent the frequency and damping factor of the i-th cisoid in the r-th mode, respectively. The cisoid is undamped when $\zeta_i^{(r)} = 0$ and damped when $\zeta_i^{(r)} < 0$. The $s_i(n)$ denotes the complex amplitude of the i-th cisoid at time instant n, and $n^{(c)}_{m_1,m_2,\ldots,m_R,n}$ is the additive colored noise component embedded in the measurement process [29–32]. Here, $N \ge 1$ is the number of snapshots in the temporal dimension. More specifically, $N=1$ and $N>1$ correspond to single-snapshot and multiple-snapshot R-D HR problems, respectively.

In tensor form, (1) is expressed as

$$\mathcal{X} = \sum_{i=1}^{d} \boldsymbol{a}(\mu_i^{(1)}) \circ \cdots \circ \boldsymbol{a}(\mu_i^{(R)}) \circ \boldsymbol{s}_i^{\mathrm{T}} + \mathcal{N}^{(c)}, \tag{2}$$

where $\mathcal{X} \in \mathbb{C}^{M_1\times M_2\times\cdots\times M_R\times N}$ is the measurement tensor that collects all noisy samples in (1), $\boldsymbol{a}(\mu_i^{(r)}) = [1, e^{\zeta_i^{(r)}+j\mu_i^{(r)}}, \ldots, e^{(M_r-1)(\zeta_1^{(r)}+j\mu_1^{(r)})}]^{\mathrm{T}}$ represents the array steering vector of the i-th source in the r-th mode, and $\boldsymbol{s}_i = [s_i(1),\ldots,s_i(N)]$ is the amplitude vector of the i-th source. In the absence of noise, $\mathcal{X}$ is composed of the sum of d components each of which corresponds to a rank-1 tensor. Therefore, it has rank d. Given the noisy measurement tensor $\mathcal{X}$, our goal is to estimate the number of signals d, which is essential to high-resolution parameter estimation.

One well known application of the above R-D HR model is angle estimation which appears in a variety of array processing applications including radar, sonar, and mobile communications. The parameters of interest include DoA (azimuth and/or elevation), DoD (azimuth and/or elevation), and Doppler shift of the targets. To estimate these parameters, shift invariant (SI) antenna arrays such as uniform linear array (ULA), uniform rectangular array (URA), uniform cubic array (UCuA) and hexagon-shaped ESPAR array [37] are widely used. A ULA can provide estimates of azimuth or elevation, while a URA can provide joint estimation of both azimuth and elevation, as shown in Fig. 1. In passive radar/sonar systems equipped with a URA at the receiver, the measurements received from d far-field narrow-band signals at azimuths θ_i and elevations α_i, $i=1,\ldots,d$, follow a 2-D undamped HR model, where the spatial frequencies $\mu_i^{(r)}$, $r=1,2$, $i=1,\ldots,d$, are given by

$$\mu_i^{(1)} = 2\pi r_1 \cos(\theta_i)\cos(\alpha_i)/\lambda, \tag{3}$$

$$\mu_i^{(2)} = 2\pi r_2 \sin(\theta_i)\cos(\alpha_i)/\lambda. \tag{4}$$

Here, r_1 and r_2 are the inter-element spacings of the receiving antenna array along the x- and y-axes, respectively, and λ denotes the carrier wavelength. In active systems with SI transmit and receive arrays, the received signals can also be formulated as an R-D HR model after appropriate preprocessing [2]. One such example arises in the bistatic MIMO radar system and will be detailed in Section 6.1.

The second important application is estimation of the parameters of the dominant multipath components in MIMO communication systems. In the parametric model of double-directional MIMO channel, each path is characterized by the following parameters: DoD, DoA, propagation delay, Doppler shift, and complex path loss [5,38]. For SI transmit and receive arrays, the channel sounding measurements after ideal low-pass filtering follow a single-snapshot R-D undamped HR model [1,4]. The parameters extracted from the channel sounding measurements can be exploited to adjust the parameters of existing channel models, to develop new realistic channel models, and even to optimize the wireless network layout of the MIMO system to guarantee high channel capacity.

Moreover, the 2-D NMR data obtained from exciting a molecular system with a 2-D radio-frequency pulse sequence can be modeled as a sum of 2-D damped cisoids [1,6]. The amplitudes, frequencies and damping factors of the 2-D harmonics provide information about the chemical shifts or resonances in a molecule, couplings between nuclear dipoles, geometric structure of the molecules and chemical exchange between two sites. In all these applications, estimating the number of signals is required prior to the use of state-of-the-art high-resolution parameter estimation techniques.

Let $\boldsymbol{A}^{(r)}$, $r=1,\ldots,R$, be the array steering matrix with the following Vandermonde structure:

$$\boldsymbol{A}^{(r)} = [\boldsymbol{a}(\mu_1^{(r)}),\ldots,\boldsymbol{a}(\mu_d^{(r)})] = \begin{bmatrix} 1 & 1 & \cdots & 1 \\ e^{(\zeta_1^{(r)}+j\mu_1^{(r)})} & e^{(\zeta_2^{(r)}+j\mu_2^{(r)})} & \cdots & e^{(\zeta_d^{(r)}+j\mu_d^{(r)})} \\ \vdots & \vdots & \ddots & \vdots \\ e^{(M_1-1)(\zeta_1^{(r)}+j\mu_1^{(r)})} & e^{(M_2-1)(\zeta_2^{(r)}+j\mu_2^{(r)})} & \cdots & e^{(M_r-1)(\zeta_d^{(r)}+j\mu_d^{(r)})} \end{bmatrix}, \tag{5}$$

and $\boldsymbol{S} = [\boldsymbol{s}_1,\ldots,\boldsymbol{s}_d]^{\mathrm{T}} \in \mathbb{C}^{d\times N}$ collect the amplitudes of all sources. In terms of r-mode products, (2) can be rewritten as

$$\mathcal{X} = \mathcal{I}_{R+1,d} \times_1 \boldsymbol{A}^{(1)} \cdots \times_R \boldsymbol{A}^{(R)} \times_{R+1} \boldsymbol{S}^{\mathrm{T}} + \mathcal{N}^{(c)}, \tag{6}$$

where $\mathcal{I}_{R+1,d}$ represents the R-D identity tensor of size $d\times d\cdots\times d$, whose elements are equal to one when $i_1 = i_2 = \cdots = i_{R+1}$ and zero otherwise.

Denoting the array steering tensor as

$$\mathcal{A} = \mathcal{I}_{R+1,d} \times_1 \boldsymbol{A}^{(1)} \times_2 \boldsymbol{A}^{(2)} \cdots \times_R \boldsymbol{A}^{(R)}, \tag{7}$$

we can express (6) in a more compact form as

$$\mathcal{X} = \mathcal{A} \times_{R+1} \boldsymbol{S}^{\mathrm{T}} + \mathcal{N}^{(c)}. \tag{8}$$

It is worth noting that our proposed R-D ESTER can be also applied in the partly uniform multidimensional HR model,

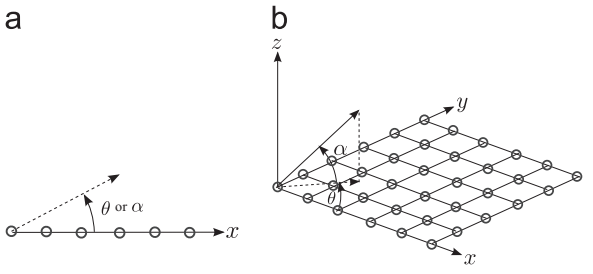

Fig. 1. Angle (azimuth and/or elevation) estimation using shift invariant arrays. (a) ULA. (b) URA.

where only part (but at least 2) of the factor matrices $\boldsymbol{A}^{(r)}$, $r=1,\ldots,R$, have a Vandermonde structure. Such a partly uniform multidimensional HR model may appear in array processing which employs a ULA/URA at the transmitter while a non-uniform antenna array at the receiver, or an antenna array with uniform spacing along one array axis but non-uniform spacing along the other axis [1].

4. Matrix based estimation error

The matrix-based ESTER [33] is an order selection rule that relies on the shift invariance property of the signal subspace. It applies in $R=1$ in which case the data model of Section 3 is reduced to the matrix form. Nevertheless, for the tensor data of $R\geq 2$, we can apply the matrix-based ESTER to one of the first R spatial dimensions for model order selection.

To this end, note that the array steering matrix in the r-th mode, namely, $\boldsymbol{A}^{(r)}$, $r=1,\ldots,R$, satisfies the so-called shift invariance equation:

$$\boldsymbol{J}_2^{(r)}\boldsymbol{A}^{(r)}=\boldsymbol{J}_1^{(r)}\boldsymbol{A}^{(r)}\cdot\boldsymbol{\Phi}^{(r)} \tag{9}$$

where $\boldsymbol{J}_1^{(r)}\in\mathbb{R}^{(M_r-1)\times M_r}$ (respectively $\boldsymbol{J}_2^{(r)}\in\mathbb{R}^{(M_r-1)\times M_r}$) is the selection matrix formed by the first (respectively last) (M_r-1) rows of an $M_r\times M_r$ identity matrix, and $\boldsymbol{\Phi}=\mathrm{diag}([e^{j\mu_1^{(r)}},e^{j\mu_2^{(r)}},\ldots,e^{j\mu_d^{(r)}}])$ is a diagonal matrix.

In practice, the array steering matrix $\boldsymbol{A}^{(r)}$ is unknown, but the singular vectors can be obtained via the singular value decomposition (SVD) of the r-th matrix unfolding of the measurement tensor $\boldsymbol{\mathcal{X}}$. Given k as the candidate value for the signal number estimate, let $\boldsymbol{U}_k^{(r)}$ collect the k dominant left singular vectors associated with the k largest singular values, and define the residual matrix as

$$\boldsymbol{E}_k^{(r)}=\boldsymbol{J}_1^{(r)}\boldsymbol{U}_k^{(r)}\cdot\boldsymbol{\Psi}_k^{(r)}-\boldsymbol{J}_2^{(r)}\boldsymbol{U}_k^{(r)}, \tag{10a}$$

where

$$\boldsymbol{\Psi}_k^{(r)}=(\boldsymbol{J}_1^{(r)}\boldsymbol{U}_k^{(r)})^{\dagger}\cdot\boldsymbol{J}_2^{(r)}\boldsymbol{U}_k^{(r)}. \tag{10b}$$

As shown in [33], for the under-enumeration case of $k<d$, the shift invariance is not satisfied, and $\|\boldsymbol{E}_k^{(r)}\|_2>0$ is the upper bound of the square error between the eigenvalues of $\boldsymbol{\Psi}_k^{(r)}$ and the closest eigenvalues of $\boldsymbol{\Psi}_d^{(r)}$. For $k=d$, as will be shown soon, $\boldsymbol{U}_d^{(r)}$ spans the same signal subspace as $\boldsymbol{A}^{(r)}$, and hence there exists a non-singular matrix $\boldsymbol{T}_r$ such that $\boldsymbol{U}_d^{(r)}=\boldsymbol{A}^{(r)}\boldsymbol{T}_r$, and $\boldsymbol{\Psi}_d^{(r)}=\boldsymbol{T}_r^{-1}\boldsymbol{\Phi}^{(r)}\boldsymbol{T}_r$ satisfies $\boldsymbol{J}_1^{(r)}\boldsymbol{U}_d^{(r)}\cdot\boldsymbol{\Psi}_d^{(r)}=\boldsymbol{J}_2^{(r)}\boldsymbol{U}_d^{(r)}$. Therefore, $\|\boldsymbol{E}_d^{(r)}\|_2=0$. For the over-enumeration case of $k>d$, $\|\boldsymbol{E}_k^{(r)}\|_2>0$ since the noise eigenvectors do not satisfy the shift invariance property. Therefore, the global minimum of zero of $\|\boldsymbol{E}_k^{(r)}\|_2$ is reached at $k=d$, and the estimated signal number, denoted by $\hat{d}_{1-\mathrm{D}}$, is obtained by minimizing the residual error:

$$\hat{d}_{1-\mathrm{D}}=\underset{k=1,\ldots,\min(M_r-2,N)}{\arg\min}\|\boldsymbol{E}_k^{(r)}\|_2^2. \tag{11}$$

5. Multidimensional estimation error

In this section, we propose two multidimensional extensions of the matrix-based ESTER by means of the HOSVD:

$$\boldsymbol{\mathcal{X}}=\boldsymbol{\mathcal{S}}\times_1\boldsymbol{U}_1\cdots\times_{R+1}\boldsymbol{U}_{R+1}, \tag{12}$$

where $\boldsymbol{\mathcal{S}}\in\mathbb{C}^{M_1\times M_2\times\cdots M_R\times N}$ is the core tensor which satisfies the all-orthogonality conditions [36] and $\boldsymbol{U}_r\in\mathbb{C}^{M_r\times M_r}$ is the unitary matrix that consists of the r-mode singular vectors.

The first extension is based on R matrix shift invariance equations each applied in one dimension and the relationship between $\boldsymbol{A}_r$ and $\boldsymbol{U}_r$, $r=1,\ldots,R$. The second extension is based on the tensor shift invariance equation, and the relationship between the array steering tensor $\boldsymbol{\mathcal{A}}$ and subspace tensor obtained from the truncated HOSVD.

5.1. R-D ESTER I

By computing the r-mode unfolding of (6) and (12), we can show that in the noiseless case, $\boldsymbol{A}^{(r)}$ and $\boldsymbol{U}_d^{(r)}$ span the same subspace. Therefore, there exists a non-singular transform matrix $\boldsymbol{T}_r\in\mathbb{C}^{d\times d}$, such that $\boldsymbol{A}^{(r)}=\boldsymbol{U}_d^{(r)}\cdot\boldsymbol{T}_r$ for all modes $r\in\mathcal{R}$, where $\mathcal{R}=\{1\leq r\leq R|M_r\geq d\}$ denotes the set of non-degenerate modes.

According to Corollary 3 of [33], in case of under-enumeration $k<d$, it holds

$$|\hat{\phi}_k^{(r)}-\phi_d^{(r)}|\leq c_r\|\boldsymbol{E}_k^{(r)}\|_2, \tag{13}$$

where $\hat{\phi}_k^{(r)}$ is an arbitrary eigenvalue of $\boldsymbol{\Psi}_k^{(r)}$, $\phi_d^{(r)}$ is an eigenvalue of $\boldsymbol{\Psi}_d^{(r)}$ that is closest to $\hat{\phi}_k^{(r)}$, and $c_r=\mathrm{cond}\{\boldsymbol{A}^{(r)}\}$ is the upper condition number which is defined as the ratio of the largest singular value of $\boldsymbol{A}^{(r)}$ to the smallest singular value of $\boldsymbol{J}_1^{(r)}\boldsymbol{A}^{(r)}$.

From (13) it follows that

$$\prod_{r=1}^{R}|\hat{\phi}_k^{(r)}-\phi_d^{(r)}|\leq\prod_{r=1}^{R}c_r\cdot\prod_{r=1}^{R}\|\boldsymbol{E}_k^{(r)}\|_2. \tag{14}$$

First, assuming that $M_1=\cdots=M_R$, we propose the R-D ESTER I for estimating the number of signals based on the following criterion:

$$\hat{d}_{R-\mathrm{D}}=\underset{k=1,\ldots,\min(M_r-2,N)}{\arg\min}E_{R-\mathrm{D}}(k), \tag{15a}$$

where

$$E_{R-\mathrm{D}}(k)=\prod_{r=1}^{R}\|\boldsymbol{E}_k^{(r)}\|_2^2. \tag{15b}$$

By applying a similar analysis to that in [33] in each mode individually, the global minimum of zero of $E_{R-\mathrm{D}}(k)$ is reached for $k=d$. For $k<d$, $E_{R-\mathrm{D}}(k)>0$ is the upper bound of the product of the square error between an arbitrary eigenvalue of $\boldsymbol{\Psi}_k^{(r)}$ and the closest eigenvalue, in least squares sense, of $\boldsymbol{\Psi}_d^{(r)}$. While for $k>d$, we also have $E_{R-\mathrm{D}}(k)>0$ since the noise eigenvectors in each mode do not satisfy the shift invariance property.

Note from (14) that the cost function $E_{R-\mathrm{D}}(k)$ in R-D ESTER I, like the matrix-based ESTER criterion, is directly associated with the variance of the biased multidimensional frequency estimates for under-enumeration. Therefore, the R-D ESTER I reserves and boost the merits of its 1-D counterpart. In particular, it enhances the robustness of the matrix-based ESTER against colored noise.

When $M_1=\cdots=M_R$ is not satisfied, a sequential MOS procedure is applied to maximize the identifiability. Specifically, we first order M_r, $r=1,\ldots,R$, in a way such that $M_{i_1}\geq M_{i_2}\geq\cdots\geq M_{i_R}$, where $i_1,i_2,\ldots,i_R$ are the ordered dimensions. Then the sequential algorithm proceeds in the following steps:

1. Start by estimating d with $\boldsymbol{U}_k^{(i_1)}$ in the first mode:
$$\hat{d}_{R-D}^{(1)}=\underset{k=1,\ldots,\min(M_{i_1}-2,N)}{\arg\min}\|\boldsymbol{E}_k^{(i_1)}\|_2^2. \tag{16a}$$
where
$$\boldsymbol{E}_k^{(i_1)}=\boldsymbol{J}_1^{(i_1)}\boldsymbol{U}_k^{(i_1)}\cdot\boldsymbol{\Psi}_k^{(i_1)}-\boldsymbol{J}_2^{(i_1)}\boldsymbol{U}_k^{(i_1)}, \tag{16b}$$
with
$$\boldsymbol{\Psi}_k^{(i_1)}=(\boldsymbol{J}_1^{(i_1)}\boldsymbol{U}_k^{(i_1)})^{\dagger}\cdot\boldsymbol{J}_2^{(i_1)}\boldsymbol{U}_k^{(i_1)}. \tag{16c}$$
2. If $\hat{d}_{R-D}^{(1)}\leq M_{i_2}-2$, we take advantage of $\boldsymbol{U}_k^{(i_2)}$ in the second mode:
$$\hat{d}_{R-D}^{(2)}=\underset{k=1,\ldots,\min(M_{i_2}-2,N)}{\arg\min}(\|\boldsymbol{E}_k^{(i_1)}\|_2\cdot\|\boldsymbol{E}_k^{(i_2)}\|_2)^2, \tag{17}$$
where $\hat{d}_{R-D}^{(2)}$ denotes the refined estimate.
3. If $\hat{d}_{R-D}^{(2)}\leq M_{i_3}-2$, $\boldsymbol{U}_k^{(i_3)}$ is exploited as well. In general, in the r-th step,
$$\hat{d}_{R-D}^{(r)}=\underset{k=1,\ldots,\min(M_{i_r}-2,N)}{\arg\min}\prod_{j=1}^{r}\|\boldsymbol{E}_k^{(i_j)}\|_2^2. \tag{18}$$
If $\hat{d}_{R-D}^{(r)}>M_{i_{r+1}}-2$ or $r=R$, stop.

Using the sequential MOS procedure, the R-D ESTER I can identify $(\max(M_1,\ldots,M_R)-2)$ signals. Note that the number of identifiable signals of the existing R-D ESTER is limited to $(\min(M_1,\ldots,M_R)-2)$ [35]. In case the lengths of spatial dimensions are distinct, the former has significantly improved identifiability over the latter.

With regard to the performance, as shown in Section 6, the superiority of the R-D ESTER I over the existing R-D ESTER scheme consists mainly in the strongly correlated colored noise environment. For low-to-moderate noise correlation levels, only slight or even no performance improvement is observed. To improve the performance for low-to-moderate noise correlation levels, we develop the second R-D ESTER based on the tensor shift invariance equation.

5.2. Proposed R-D ESTER II

As shown in [15], the r-mode matrix unfoldings of $\mathcal{A}$, $r=1,\ldots,R$, satisfy the following shift invariance equations:
$$\begin{aligned}&\mathcal{A}\times_1\boldsymbol{J}_1^{(1)}\times_{R+1}\boldsymbol{\Phi}^{(1)}=\mathcal{A}\times_1\boldsymbol{J}_2^{(1)},\\&\mathcal{A}\times_2\boldsymbol{J}_1^{(2)}\times_{R+1}\boldsymbol{\Phi}^{(2)}=\mathcal{A}\times_2\boldsymbol{J}_2^{(2)},\cdots\\&\mathcal{A}\times_R\boldsymbol{J}_1^{(R)}\times_{R+1}\boldsymbol{\Phi}^{(R)}=\mathcal{A}\times_R\boldsymbol{J}_2^{(R)}.\end{aligned} \tag{19}$$

From (19), it follows that (See Appendix A):
$$\mathcal{A}\times_1\boldsymbol{J}_1^{(1)}\cdots\times_R\boldsymbol{J}_1^{(R)}\times_{R+1}\prod_{r=1}^{R}\boldsymbol{\Phi}^{(r)}=\mathcal{A}\times_1\boldsymbol{J}_2^{(1)}\cdots\times_R\boldsymbol{J}_2^{(R)}. \tag{20}$$
Eq. (20) is an extension of the matrix shift invariance equation in (9) to the tensor case, and hence is referred to as the tensor shift invariance equation.

Since the array steering tensor $\mathcal{A}$ is not available, the HOSVD described in (12) is applied to find the subspace tensor. After applying the low rank approximation of order k to (12), the subspace tensor $\mathcal{U}_k$ is identified as
$$\mathcal{U}_k=\mathcal{S}_k\times_1\boldsymbol{U}_k^{(1)}\cdots\times_R\boldsymbol{U}_k^{(R)}, \tag{21}$$
where $\mathcal{S}_k\in\mathbb{C}^{p_1\times\cdots\times p_R\times k}$, and $\boldsymbol{U}_k^{(r)}\in\mathbb{C}^{M_r\times p_r}$, with $p_r=\min(M_r,k)$ for $r=1,\ldots,R$. In the noiseless case and for $k=d$, it is shown that $\mathcal{A}$ and $\mathcal{U}_d$ are related by [15]
$$\mathcal{A}=\mathcal{U}_d\times_{R+1}\boldsymbol{T}, \tag{22}$$
where $\boldsymbol{T}$ is a non-singular matrix.

Substituting (22) into (20), we obtain
$$\begin{aligned}&\mathcal{U}_d\times_{R+1}\boldsymbol{T}\times_1\boldsymbol{J}_1^{(1)}\cdots\times_R\boldsymbol{J}_1^{(R)}\times_{R+1}\prod_{r=1}^{R}\boldsymbol{\Phi}^{(r)}\\&\quad=\mathcal{U}_d\times_{R+1}\boldsymbol{T}\times_1\boldsymbol{J}_2^{(1)}\cdots\times_R\boldsymbol{J}_2^{(R)},\end{aligned} \tag{23}$$
which can be rewritten as
$$\mathcal{U}_d\times_1\boldsymbol{J}_1^{(1)}\cdots\times_R\boldsymbol{J}_1^{(R)}\times_{R+1}\boldsymbol{T}^{-1}\prod_{r=1}^{R}\boldsymbol{\Phi}^{(r)}\boldsymbol{T}=\mathcal{U}_d\times_1\boldsymbol{J}_2^{(1)}\cdots\times_R\boldsymbol{J}_2^{(R)}. \tag{24}$$
Let
$$\boldsymbol{\Psi}_d^{(G)}=\boldsymbol{T}^{-1}\prod_{r=1}^{R}\boldsymbol{\Phi}^{(r)}\boldsymbol{T}, \tag{25}$$
and
$$\begin{aligned}&\mathcal{U}_k^{\downarrow}=\mathcal{U}_k\times_1\boldsymbol{J}_1^{(1)}\cdots\times_R\boldsymbol{J}_1^{(R)}=\mathcal{U}_k\overset{R}{\underset{r=1}{\times}}{}_r\boldsymbol{J}_1^{(r)},\\&\mathcal{U}_k^{\uparrow}=\mathcal{U}_k\times_1\boldsymbol{J}_2^{(1)}\cdots\times_R\boldsymbol{J}_2^{(R)}=\mathcal{U}_k\overset{R}{\underset{r=1}{\times}}{}_r\boldsymbol{J}_2^{(r)},\end{aligned} \tag{26}$$
where the operator $\times_{r=1}^{R}$ denotes a compact representation of R r-mode products between a tensor and R matrices. Eq. (24) can be expressed in a more compact form as
$$\mathcal{U}_d^{\downarrow}\times_{R+1}\boldsymbol{\Psi}_d^{(G)}=\mathcal{U}_d^{\uparrow}. \tag{27}$$
Applying the $(R+1)$-mode unfolding to the tensors on both sides of (27), we obtain
$$\boldsymbol{\Psi}_d^{(G)}\cdot[\mathcal{U}_d^{\downarrow}]_{(R+1)}=[\mathcal{U}_d^{\uparrow}]_{(R+1)}. \tag{28}$$
Therefore
$$\boldsymbol{\Psi}_d^{(G)}=[\mathcal{U}_d^{\uparrow}]_{(R+1)}\cdot([\mathcal{U}_d^{\downarrow}]_{(R+1)})^{\dagger}. \tag{29}$$
Note that when $k\neq d$, (24) does not hold. Therefore, the number of signals can be estimated as
$$\hat{d}_{R-D}=\underset{k=1,\ldots,\min(\max(M_1,\ldots,M_R)-2,N)}{\arg\min}E_{R-D}(k), \tag{30a}$$
where
$$E_{R-D}(k)=\left\|\mathcal{U}_k\overset{R}{\underset{r=1}{\times}}{}_r\boldsymbol{J}_1^{(r)}\times_{R+1}\boldsymbol{\Psi}_k^{(G)}-\mathcal{U}_k\overset{R}{\underset{r=1}{\times}}{}_r\boldsymbol{J}_2^{(r)}\right\|_F^2, \tag{30b}$$

is the error function to be minimized, with

$$\boldsymbol{\Psi}_k^{(\mathrm{G})} = \left[\boldsymbol{\mathcal{U}}_k \underset{r=1}{\overset{R}{\times}}{}_r\boldsymbol{J}_2^{(r)}\right]_{(R+1)} \cdot \left(\left[\boldsymbol{\mathcal{U}}_k \underset{r=1}{\overset{R}{\times}}{}_r\boldsymbol{J}_1^{(r)}\right]_{(R+1)}\right)^{\dagger}. \tag{30c}$$

It is easy to verify that $E_{R-\mathrm{D}}(k) > 0$ for $k < d$ and $k > d$ in the absence of noise.

Note that the original R-D ESTER in [35] has a similar tensor form to the proposed R–D ESTER II. However, the former is based on a shift invariance equality that is formed by empirically combining the shift invariance equations in individual dimensions, and that is of similar form to Eq. (1) except that U_d is replaced by one with an identity core. In the latter, by means of the tensor shift invariance equation that incorporates the core tensor of the truncated HOSVD, a more reliable performance is ensured. In addition, similar to R-D ESTER I, the number of identifiable signals of the R-D ESTER II is increased up to $(\max(M_1,\ldots,M_R)-2)$ for $N \geq \max(M_1,\ldots,M_R)-2$, which is a considerable improvement over the original R-D ESTER when the lengths of spatial dimensions are quite different.

As shown in Section 6, for a wide range of low-to-moderate noise correlation levels, the R-D ESTER II outperforms the original R-D ESTER as well as R-D ESTER I. However, for high noise correlation levels, its performance degrades sharply, showing a weakened robustness against colored noise. This may stem from its failure (this also applies to the original R-D ESTER) to preserve the inherent structure of the matrix based ESTER. To see this, note that the cost function in the matrix based ESTER is the spectral norm of the residual matrix $\boldsymbol{E}(k)$, which for the under-enumeration case is the upper bound of the variance of the biased frequency estimates. Both the R-D ESTER II and original R-D ESTER lose such a connotation in a sense that the relationship between their cost functions and the errors of the estimated eigenvalues is unclear. Consequently, for strongly correlated colored noise scenarios, they perform not as well as the R-D ESTER I.

5.3. Computational complexity

Two dominant calculations in the ESTER are SVD and Moore–Penrose pseudo inverse. Both operations involve $O(P^2Q)$ flops for a $P \times Q$ $(P \leq Q)$ matrix, provided that the Moore–Penrose pseudo inverse is also calculated based on the SVD. For R-D ESTER I, the computational load is equal to or less than that of R matrix based ESTERs each applied in a matrix unfolding of the measurement tensor. For each matrix-based ESTER, once the singular vectors have been obtained via the SVD of the r-mode unfolding, an efficient algorithm derived in [33] can be used to recursively calculate the residual matrix for all $k = 1,\ldots,M_r-2$. Such an algorithm involves $6M_rk$ flops for each k, so that the overall complexity is $3M_r(M_r-2)^2$. In the original R-D ESTER and R-D ESTER II, in addition to R SVDs of r-mode $(r = 1,\ldots,R)$ unfoldings of the measurement tensor, the subspace tensor $\boldsymbol{\mathcal{U}}_k$ needs to be calculated for all k. For the R-D ESTER II, additional flops are required to compute the core tensor $\boldsymbol{\mathcal{S}}$ of HOSVD. The computational complexity in terms of number of required flops of the proposed two R-D ESTER methods and original R-D ESTER is summarized in Table 1, where $M = \prod_{r=1}^{R} M_r$. It shows that the matrix-based R-D ESTER I requires much smaller number of flops than that required in the tensor-based R-D ESTER II and original R-D ESTER, which have the same order of complexity.

6. Simulation results

We present simulation results demonstrating the performance of the proposed R-D ESTER schemes. To simulate the correlation in multidimensional colored noise, we use the following noise generating model [39,40,35]:

$$\boldsymbol{\mathcal{N}}^{(\mathrm{C})} = \boldsymbol{\mathcal{N}} \times_1 \boldsymbol{L}_1 \times_2 \boldsymbol{L}_2 \cdots \times_R \boldsymbol{L}_R. \tag{31}$$

where $\boldsymbol{\mathcal{N}} \in \mathbb{C}^{M_1 \times \cdots \times M_R \times N}$ is a white noise tensor collecting uncorrelated zero-mean circularly symmetric complex Gaussian (ZMCSCG) noise samples with variance σ_n^2, and $\boldsymbol{L}_r \in \mathbb{C}^{M_r \times M_r}$, $r = 1,\ldots,R$, is the correlation factor in the r-th dimension of the colored noise tensor. The signal-to-noise ratio (SNR) is defined as

$$\mathrm{SNR} = \frac{\|\boldsymbol{\mathcal{A}} \times_{R+1} \boldsymbol{S}^{\mathrm{T}}\|_{\mathrm{F}}^2}{\prod_{r=1}^{R} M_r N \sigma_z^2}. \tag{32}$$

As in [35], the colored noise is modeled as a first-order autoregressive process:

$$n_{m+1}^{(\mathrm{C})} = \rho_r \cdot n_m^{(\mathrm{C})} + \sqrt{1-|\rho_r|^2} \cdot n_{m+1}, \tag{33}$$

such that the noise covariance matrix $\boldsymbol{C}_r = \boldsymbol{L}_r \cdot \boldsymbol{L}_r^{\mathrm{H}}$, $r = 1,\ldots,R$, is a function of a single variable, namely, the correlation coefficient ρ_r only. For example, when $M_r = 3$, $\boldsymbol{C}_r$ has the following structure:

$$\boldsymbol{C}_r = \begin{bmatrix} 1 & \rho_r^* & (\rho_r^*)^2 \\ \rho_r & 1 & \rho_r^* \\ \rho_r^2 & \rho_r & 1 \end{bmatrix}. \tag{34}$$

It is worth noting that for other types of noise correlation models, similar simulation results are observed.

The performance measure is the PoD, i.e., $\Pr(\hat{d} = d)$. The following schemes are used as the benchmark: the R-D MDL/AIC [22], R-D RMT [23] with a constant confidence level of $\alpha = 10^{-2}$, 1-D ESTER applied to each mode unfolding of the measurement data, and original R-D ESTER [35].

Table 1
Number of flops required in the proposed R-D ESTER methods and original R-D ESTER.

Proposed R-D ESTER I	Proposed R-D ESTER II	Original R-D ESTER
$O[\sum_{r=1}^{R} 3M_r(M_r-2)^2]$	$O[MN(\sum_{r=1}^{R} M_r+N)+RMM_r^2]$	$O[MN(\sum_{r=1}^{R} M_r+N)+MM_r^2]$

6.1. Simulation scenario I: source localization in multiple-pulses, bistatic MIMO radar

The MIMO radar is characterized by using multiple antennas to simultaneously transmit linearly independent waveforms and by utilizing multiple antennas to receive the reflected signals. In the bistatic MIMO radar configuration [2], the transmit and receive arrays are separately located by a considerable distance. The received signals are multiplied by the inversion of the waveform matrix (matched filtering) in order to achieve waveform diversity. When a ULA/URA is used at both the transmitter and receiver, the matched-filter output corresponds to an R-D undamped HR model [2], namely, (1), where the spatial frequency $\mu_i^{(r)}$, $r=1,\ldots,R$, is expressed as a function of the DoA (azimuth and/or elevation) and DoD (azimuth and/or elevation) of the i-th target, and $s_i(n)=\beta_{i,n}e^{j(n-1)\chi_i}$, $n=1,\ldots,N$. Here, N is the number of pulses in each coherent processing interval (CPI), $\beta_{i,n}$ is the RCS coefficient of the i-th target, and χ_i is the Doppler frequency determined by

$$\chi_i=2\pi v_i T_p/\lambda, \tag{35}$$

where v_i is the velocity of the i-th target in meters per second, T_p is the pulse duration in seconds, and $\lambda=3\cdot 10^8/f_c$ is the wavelength, with f_c being the carrier frequency.

We consider the scenario where each CPI comprises multiple consecutive pulse periods, namely, $N>1$. In the Swerling I target model, the RCSs of all targets are constant during the CPI, which means that $\beta_{i,n}=\beta_i$, $n=1,\ldots,N$. Therefore, $\boldsymbol{S}$ is a Vandermonde matrix as well, and the multiple-snapshot R-D undamped HR model can be interpreted as an equivalent single-snapshot $(R+1)$-D undamped HR model. While in the Swerling II target model, the target RCS is varying from pulse to pulse in a CPI.

In consistent with [2], the specific parameter settings are set as follows. The transmitted waveforms are chosen from the first M_T rows of a 64×64 Hadamard matrix, where M_T is the number of transmit antennas. We assign $T_p=5\times 10^{-6}$ and f_c=1 GHz. The ULA/URA has an inter-element spacing of half the wavelength. The azimuth and elevation are assumed to be drawn from a uniform distribution in $[-\pi,\pi]$ and $[-\pi/2,\pi/2]$, respectively. The Kronecker colored noise is added to the noise-free received signal prior to matched filtering. For simplicity but without loss of generality, we assume that the noise correlation is present in all dimensions except the temporal dimension. The number of pulses in each CPI is set as N=20. The RCS coefficients $\beta_{i,n}$ are assumed to be drawn from a complex Gaussian distribution with zero mean and variance $\sigma^2_{\beta_i}=0.3+0.1(i-1)$, $i=1,\ldots,d$. For each SNR, the PoD is computed from 1000 independent Monte Carlo runs.

6.1.1. Swerling II target model

First, we consider a scenario where both the transmitter and receiver employ an eight-element ULA. The matched-filter output follows a multiple-snapshot 2-D undamped HR model [2], namely, (1) with R=2, $M_1=M_2=8$ and N=20. The spatial frequencies $\mu_i^{(r)}$, r=1,2, $i=1,\ldots,d$, are given by

$$\mu_i^{(1)}=\pi\cos(\theta_i^{(R)}), \tag{36}$$

$$\mu_i^{(2)}=\pi\cos(\theta_i^{(T)}), \tag{37}$$

where $\theta_i^{(R)}$ and $\theta_i^{(T)}$ are the azimuth of arrival and departure of the i-th source, respectively.

In Fig. 2, the PoDs versus SNR of different order selection rules are compared for d=3 sources, where the correlation coefficients of the colored noise are set as $\rho_1=\rho_2=0.125$. We see that R-D ESTER I has almost the same PoD as the original one, while R-D ESTER II significantly outperforms [35]. In Fig. 3, the number of sources is increased to 5, and the improvement of R-D ESTER II over the original one is more obvious. Note that the PoDs of R-D ESTER methods are higher than those of all ESTER 1, ESTER 2, and ESTER 3. Note also that the R-D MDL/AIC and R-D RMT cannot attain a PoD of 1 even at high SNRs due to over-enumeration.

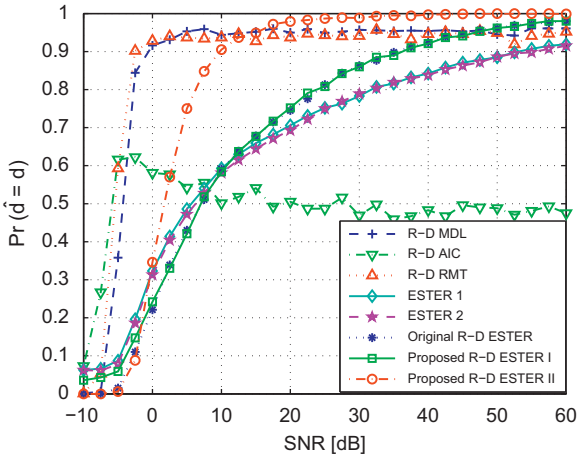

Fig. 2. PoD versus SNR of Swerling II targets for source localization in multiple-pulse, bistatic MIMO radar system. R=2, $M_1=M_2=8$, N=20, d=3. The noise correlation coefficients are $\rho_1=\rho_2=0.125$.

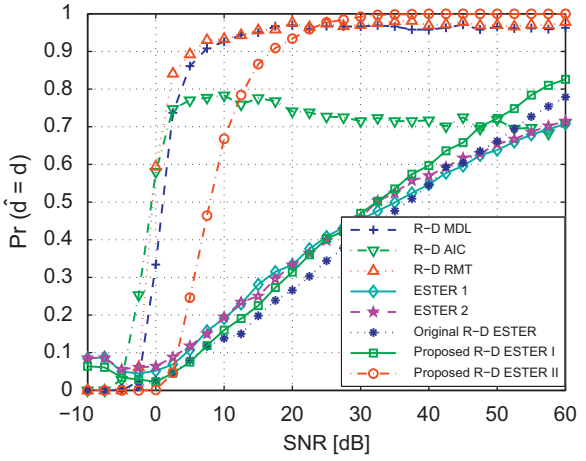

Fig. 3. PoD versus SNR of Swerling II targets for source localization in multiple-pulse, bistatic MIMO radar system. The parameter settings are the same as those in Fig. 2 except that d=5.

In Fig. 4, we have the same scenario as in Fig. 3, except that instead of a low noise correlation level, here we use a high noise correlation level of $\rho_1 = \rho_2 = 0.8$. We see that R-D ESTER I outperforms [35] as well as all ESTER 1, ESTER 2, and ESTER 3, regardless of the noise level, while R-D ESTER II performs poorly and is inferior to [35]. For such strongly correlated colored noise, the R-D MDL/AIC/RMT that is designed for white noise totally fail.

Next, we consider a scenario where the transmitter employs a 6-element ULA, while the receiver employs a 6×6-element URA. The matched-filter output follows a multiple-snapshot 3-D undamped HR model [2], namely, (1) with $R=3$, $M_1 = M_2 = M_3 = 6$ and $N=20$. The spatial frequencies $\mu_i^{(r)}$, $r = 1,2,3$, $i = 1, \ldots, d$, are determined by

$$\mu_i^{(1)} = \pi \cos(\theta_i^{(\mathrm{R})}) \cos(\alpha_i^{(\mathrm{R})}), \tag{38}$$

$$\mu_i^{(2)} = \pi \sin(\theta_i^{(\mathrm{R})}) \cos(\alpha_i^{(\mathrm{R})}), \tag{39}$$

$$\mu_i^{(3)} = \pi \cos(\theta_i^{(\mathrm{T})}), \tag{40}$$

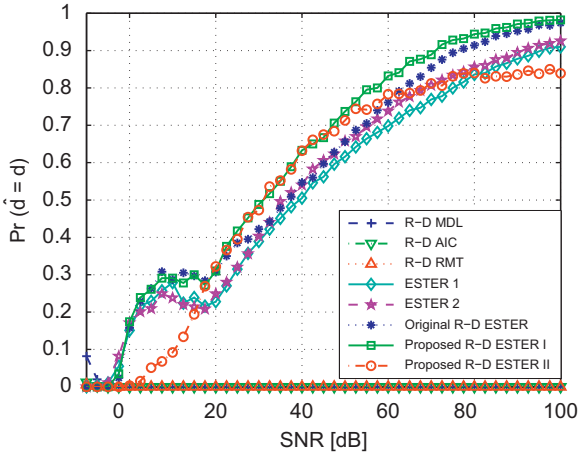

Fig. 4. PoD versus SNR of Swerling II targets for source localization in multiple-pulse, bistatic MIMO radar system. The parameter settings are the same as those in Fig. 3 except that $\rho_1 = \rho_2 = 0.8$.

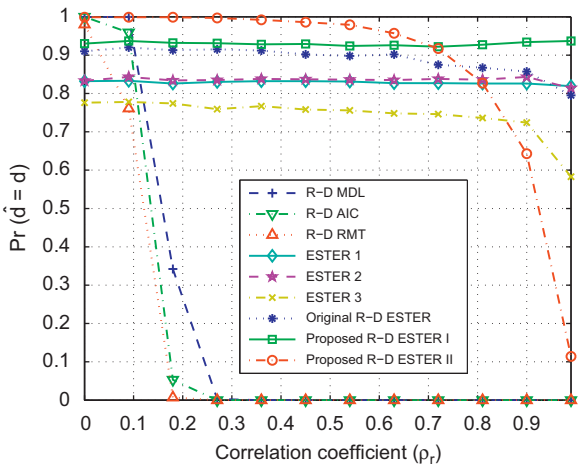

Fig. 5. PoD versus noise correlation level ρ_r in colored noise environment. $R=3$, $M_1 = M_2 = M_3 = 6$, $N=20$, $d=3$. SNR=30 dB.

where $\theta_i^{(\mathrm{R})}$, $\alpha_i^{(\mathrm{R})}$ and $\theta_i^{(\mathrm{T})}$ are the azimuth of arrival, elevation of arrival and azimuth of departure, respectively.

In Fig. 5, the order selection rules are evaluated for various noise correlation levels at a fixed SNR=30 dB and $d=3$. Here, the correlation coefficients along different dimensions are equal to each other and vary from 0 to 0.999. We see that with the increase of the noise correlation levels, the R-D ESTER I and 1-D ESTERs maintain constant detection performance whereas all other schemes suffer performance degradation to a certain extent. While the original R-D ESTER experiences a slight performance degradation only for high correlation levels, the R-D MDL/AIC/RMT drops sharply in performance and totally fails for $\rho_r > 0.3$. For the R-D ESTER II, it performs best for a wide range of low-to-moderate noise correlation levels of $\rho_r < 0.7$. However, for high noise correlation levels, it drops sharply in PoD and is inferior to the R-D ESTER I and [35] when $\rho_r > 0.8$ i. This indicates that the order of robustness against colored noise is: R-D ESTER I

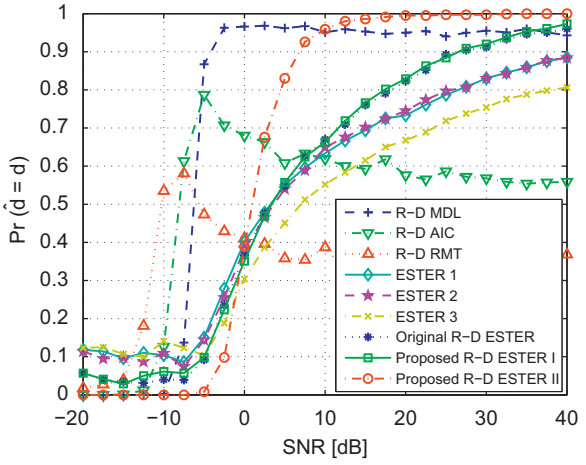

Fig. 6. PoD versus SNR of Swerling II targets for source localization in multiple-pulse, bistatic MIMO radar system. $R=3$, $M_1 = M_2 = M_3 = 6$, $N=20$, $d=3$. The noise correlation coefficients are $\rho_1 = \rho_2 = \rho_3 = 0.125$.

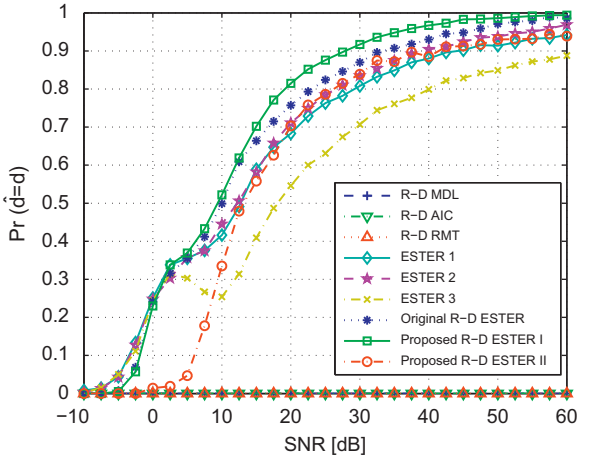

Fig. 7. PoD versus SNR of Swerling II targets for source localization in multiple-pulse, bistatic MIMO radar system. The parameter settings are the same as those in Fig. 6 except that $\rho_1 = \rho_2 = \rho_3 = 0.8$.

(1-D ESTERs) > original R-D ESTER > R-D ESTER $rmII \gg$ R-D MDL/AIC/RMT.

In Fig. 6, the correlation coefficients of the colored noise are fixed as $\rho_1=\rho_2=\rho_3=0.125$ while the SNR varies. We see that the R-D ESTER II performs best and remarkably outperforms [35] as well as other methods. In Fig. 7, the noise correlation level is increased to $\rho_1=\rho_2=\rho_3=0.8$. In such a strongly correlated colored noise scenario, the R-D ESTER I is instead the best performing method. These observations are consistent with those obtained in Figs. 2–4 and Fig. 5, which implies that the R-D ESTER I has strongest robustness, while the R-D ESTER II is less robust against colored noise but is optimal for weakly-to-moderately correlated colored noise scenarios.

Next, we change the antenna array sizes such that $M_1=7$, $M_2=5$, $M_3=9$. For such a 3-D array of distinct sizes, both R-D ESTER schemes can identify $M_1-2=7$ sources, while the original R-D ESTER can only identify $M_2-2=3$ sources.

In Figs. 8 and 9, different order selection rules are assessed for five sources at low-to-moderate and high noise correlation levels, respectively. We see that the original R-D ESTER fails to work. In contrast, the R-D ESTER I and R-D ESTER II respectively works well in weakly-to-moderately and strongly correlated colored noise scenarios, and attain a PoD of 1 at sufficiently high SNRs.

Finally, we consider a scenario where both the transmitter and receiver employ a 5×5-element URA. The matched-filter output obeys a multiple-snapshot 4-D undamped HR model [2], namely, (1) with $R=4$, $M_1=M_2=M_3=M_4=5$ and $N=20$. The spatial frequencies $\mu_i^{(r)}$, $r=1,2,3,4$, $i=1,\ldots,d$, are given by

$$\mu_i^{(1)}=\pi\cos(\theta_i^{(\mathrm{R})})\cos(\alpha_i^{(\mathrm{R})}), \tag{41}$$

$$\mu_i^{(2)}=\pi\sin(\theta_i^{(\mathrm{R})})\cos(\alpha_i^{(\mathrm{R})}), \tag{42}$$

$$\mu_i^{(3)}=\pi\cos(\theta_i^{(\mathrm{T})})\cos(\alpha_i^{(\mathrm{T})}), \tag{43}$$

$$\mu_i^{(4)}=\pi\sin(\theta_i^{(\mathrm{T})})\cos(\alpha_i^{(\mathrm{T})}), \tag{44}$$

where $\theta_i^{(\mathrm{R})}$, $\alpha_i^{(\mathrm{R})}$, $\theta_i^{(\mathrm{T})}$ and $\alpha_i^{(\mathrm{T})}$ denote the azimuth of arrival, elevation of arrival, azimuth of departure and elevation of departure, respectively.

In Figs. 10 and 11, different order selection rules are assessed for two sources at low-to-moderate and high noise correlation levels, respectively. Again, the R-D ESTER I performs comparably to or better than the original R-D ESTER for all noise correlation levels. For R-D ESTER II, it is superior to the original R-D ESTER by a considerable margin for low-to-moderate noise correlation levels, while inferior to the latter for high noise correlation levels. This confirms the weaker robustness of the R-D ESTER II with respect to the R-D ESTER I and original R-D ESTER methods.

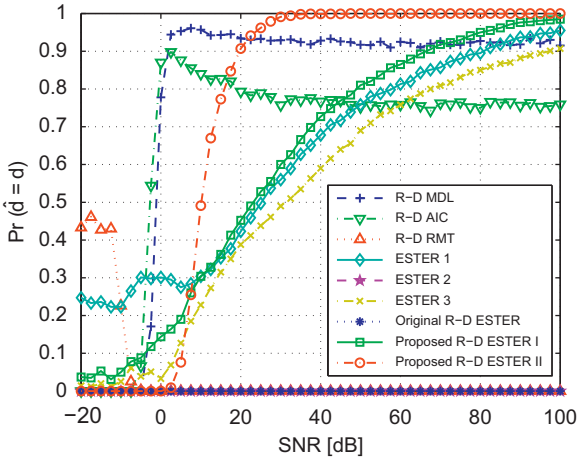

Fig. 8. PoD versus SNR of Swerling II targets for source localization in multiple-pulse, bistatic MIMO radar system. $R=3, M_1=7, M_2=5, M_3=9$, $N=20$, $d=5$. The noise correlation coefficients are $\rho_1=\rho_2=\rho_3=0.125$.

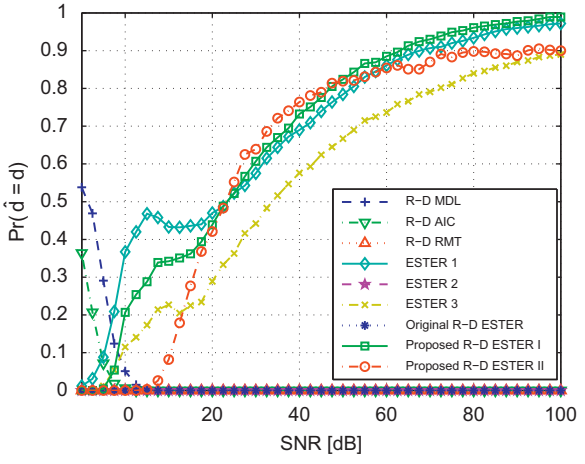

Fig. 9. PoD versus SNR of Swerling II targets for source localization in multiple-pulse, bistatic MIMO radar system. $R=3, M_1=7, M_2=5, M_3=9$, $N=20$, $d=5$. The noise correlation coefficients are $\rho_1=\rho_2=\rho_3=0.8$.

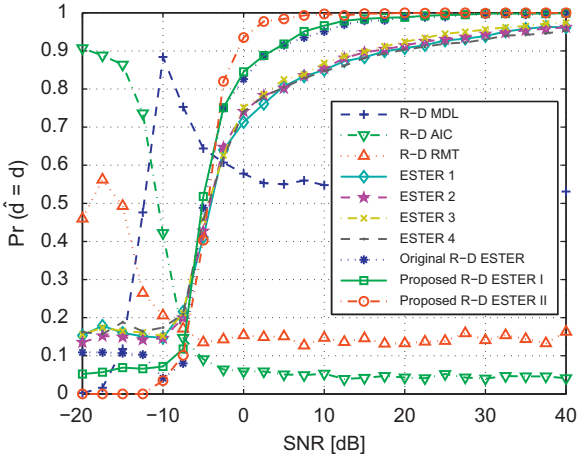

Fig. 10. PoD versus SNR of Swerling II targets for source localization in multiple-pulse, bistatic MIMO radar system. $R=4, M_1=M_2=M_3=M_4=5$. The number of pulse in each CPI is $N=20$. $d=2$. The noise correlation coefficients are $\rho_1=\rho_2=\rho_3=\rho_4=0.125$.

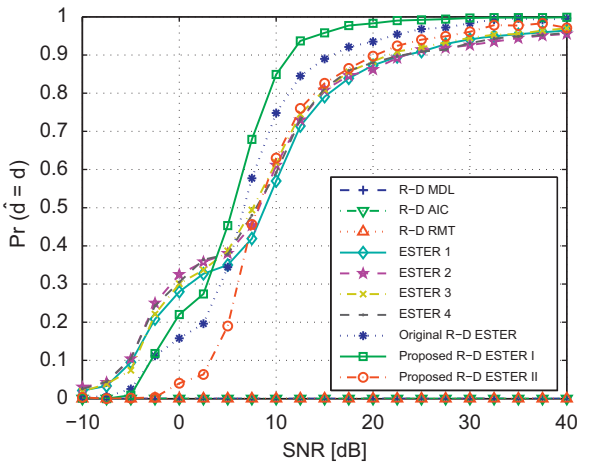

Fig. 11. PoD versus SNR of Swerling II targets for source localization in multiple-pulse, bistatic MIMO radar system. The parameter settings are the same as those in Fig. 10 except that $\rho_1=\rho_2=\rho_3=\rho_4=0.8$.

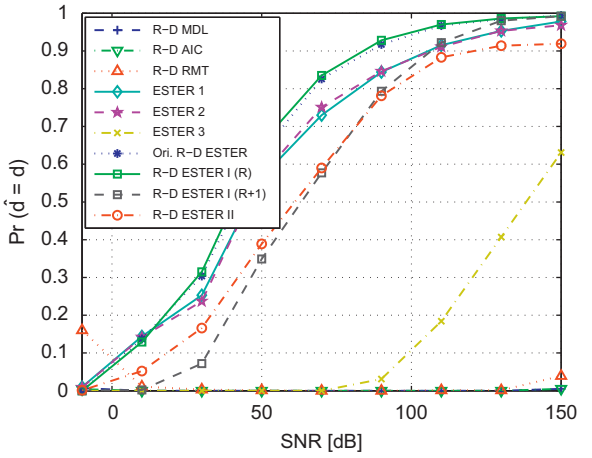

Fig. 12. PoD versus SNR of Swerling I targets for source localization in multiple-pulse, bistatic MIMO radar system. $R=2$, $M_1=M_2=8$. The number of pulse in each CPI is $N=8$. $d=5$.

6.1.2. Swerling I target model

Consider the scenario where both the transmitter and receiver employ an eight-element ULA, with eight pulses in each CPI. The matched-filter output corresponds to a single-snapshot 3-D undamped HR model [2], namely, (1) with $R=3$, $M_1=M_2=M_3=8$ and $s_i(n)=\beta_i$. The spatial frequencies $\mu_i^{(r)}$, $r=1,2,3$, $i=1,\ldots,d$, are given by

$$\mu_i^{(1)}=\pi\cos(\theta_i^{(\mathrm{R})}), \tag{45}$$

$$\mu_i^{(2)}=\pi\cos(\theta_i^{(\mathrm{T})}), \tag{46}$$

$$\mu_i^{(3)}=\chi_i, \tag{47}$$

where χ_i is the Doppler shift determined by (35). As in [2], we assume that the target velocity is uniformly distributed in $[0,\lambda/(10\cdot 2T_p)]=[0,3000]$, such that $\chi_i\ll\pi$ is uniformly distributed in $[0,\pi/10]$.

Since $\boldsymbol{A}^{(3)}$ has a Vandermonde structure, the R-D ESTER I can exploit the third matrix unfolding as well. For ease of distinction, we denote the R-D ESTER I that exploits the third unfolding and the one without exploiting the third unfolding as "R-D ESTER I $(R+1)$" and "R-D ESTER I (R)", respectively. In Fig. 12, we plot the result for five sources and strongly correlated noise of $\rho_1=\rho_2=\rho_3=0.8$. We see that the ESTER 3 that applies to the third unfolding performs poorly due to frequent under-enumeration and the "R-D ESTER I $(R+1)$" is inferior to "R-D ESTER I (R)". This is not unexpected, considering that the Doppler shifts of different sources are so small that $\boldsymbol{A}^{(3)}$ is nearly rank deficient. Therefore, in such a scenario, it is preferred not to use the third unfolding.

6.2. Simulation scenario II: Wireless channel sounding

Consider a stationary wireless scenario where there is no Doppler shift. When uniform linear transmit and receive arrays are employed, the baseband-equivalent channel sounding measurements after ideal low-pass filtering follow a single-snapshot 3-D undamped HR model, where the frequencies $\mu_i^{(r)}$, $r=1,2,3$, $i=1,\ldots,d$, in (1) are given by [1,4]

$$\mu_i^{(1)}=\pi\cos(\theta_i^{(\mathrm{R})}), \tag{48}$$

$$\mu_i^{(2)}=\pi\cos(\theta_i^{(\mathrm{T})}), \tag{49}$$

$$\mu_i^{(3)}=2\pi\tau_i/N. \tag{50}$$

Here $\theta_i^{(\mathrm{R})}$, $\theta_i^{(\mathrm{T})}$ and τ_i are the azimuth of arrival, azimuth of departure and propagation delay measured in samples of the i-th source, respectively. The azimuths are assumed to be drawn from a uniform distribution in $[-\pi,\pi]$, and the propagation delay is assumed to be drawn from a uniform distribution in $[0,N-1]$.

In Figs. 13 and 14, different order selection rules are assessed for five sources at low-to-moderate and high noise correlation levels, respectively. In contrast to Fig. 12, since $\boldsymbol{A}^{(3)}$ is no longer a rank deficient matrix, the "R-D ESTER I $(R+1)$" that exploits the third unfolding is

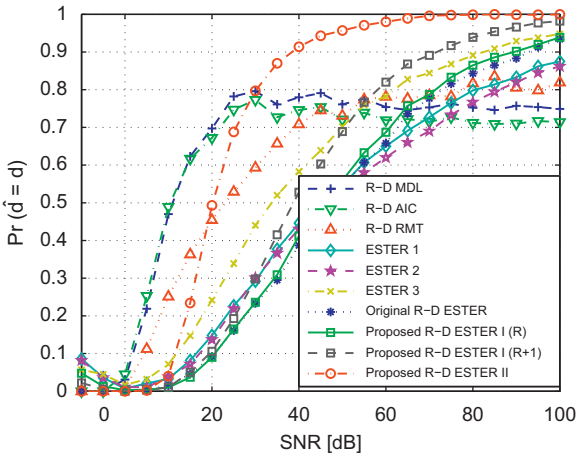

Fig. 13. PoD versus SNR for channel parameter estimation from multi-dimensional channel sounding measurements. The parameter settings are the same as those in Fig. 12.

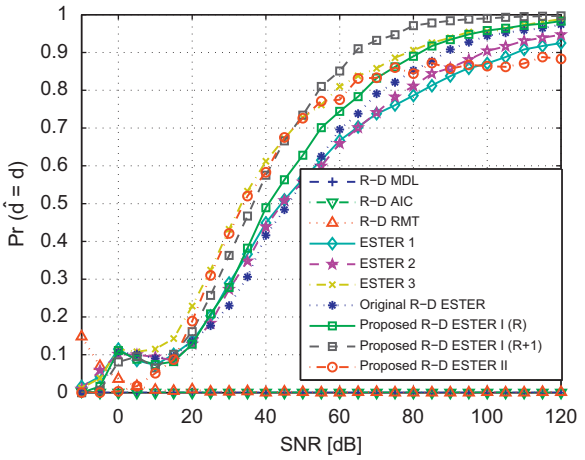

Fig. 14. PoD versus SNR for channel parameter estimation from multi-dimensional channel sounding measurements. The parameter settings are the same as those in Fig. 12.

superior to "*R*-D ESTER I (*R*)" without exploiting the third unfolding.

7. Conclusion

We propose two multidimensional extensions of the subspace based 1-D estimation error (ESTER) rule for estimating the number of multidimensional signals in colored noise. Our schemes take into account the multi-dimensional structure of the data and hence considerably outperforms the matrix-based 1-D ESTER. The *R*-D ESTER I combines *R* sets of eigenvectors of the higher-order SVD of the measurement tensor based on *R* matrix shift invariance equations in all modes. It preserves the inherent structure of the matrix-based ESTER with enhanced robustness against colored noise, and outperforms the state-of-the-art *R*-D ESTER scheme particularly in strongly correlated colored noise environment. To further improve the performance at low-to-moderate noise correlation levels, the *R*-D ESTER II is developed based on the tensor shift invariance equation. It is the best performing method for a wide range of weakly and moderately correlated colored noise scenarios. However, for high noise correlation levels, it is inferior to the existing schemes. Both of our proposed extensions can identify considerably more signals the existing *R*-D ESTER scheme when the spatial dimension lengths are distinct from each other.

Appendix A

In order to prove the global equation in (20), we apply the method of induction. For $r=1$, it holds that

$$\mathcal{A}\times_1 \boldsymbol{J}_1^{(1)}\times_{R+1}\boldsymbol{\Phi}^{(1)} = \mathcal{A}\times_1 \boldsymbol{J}_2^{(1)}. \tag{A.1}$$

Suppose for a certain $r \geq 1$, we have

$$\mathcal{A}\times_1 \boldsymbol{J}_1^{(1)}\cdots\times_r \boldsymbol{J}_1^{(r)}\times_{R+1}\prod_{i=1}^{r}\boldsymbol{\Phi}^{(i)} = \mathcal{A}\times_1 \boldsymbol{J}_2^{(1)}\cdots\times_r \boldsymbol{J}_2^{(r)}. \tag{A.2}$$

Then for $r+1$,

$$\begin{aligned}
&\mathcal{A}\times_1 \boldsymbol{J}_2^{(1)}\cdots\times_r \boldsymbol{J}_2^{(r)}\times_{r+1}\boldsymbol{J}_2^{(r+1)}\\
&= \left(\mathcal{A}\times_1 \boldsymbol{J}_1^{(1)}\cdots\times_r \boldsymbol{J}_1^{(r)}\times_{R+1}\prod_{i=1}^{r}\boldsymbol{\Phi}^{(i)}\right)\times_{r+1}\boldsymbol{J}_2^{(r+1)}\\
&= (\mathcal{A}\times_{r+1}\boldsymbol{J}_2^{(r+1)})\times_1 \boldsymbol{J}_1^{(1)}\cdots\times_r \boldsymbol{J}_1^{(r)}\times_{R+1}\prod_{i=1}^{r}\boldsymbol{\Phi}^{(i)}\\
&= (\mathcal{A}\times_{r+1}\boldsymbol{J}_1^{(r+1)}\times_{R+1}\boldsymbol{\Phi}^{(r+1)})\times_1 \boldsymbol{J}_1^{(1)}\cdots\times_r \boldsymbol{J}_1^{(r)}\times_{R+1}\prod_{i=1}^{r}\boldsymbol{\Phi}^{(i)}\\
&= \mathcal{A}\times_1 \boldsymbol{J}_1^{(1)}\cdots\times_r \boldsymbol{J}_1^{(r)}\times_{r+1}\boldsymbol{J}_1^{(r+1)}\times_{R+1}\prod_{r=1}^{r+1}\boldsymbol{\Phi}^{(r)}.
\end{aligned} \tag{A.3}$$

This completes the proof.

References

[1] M. Pesavento, Fast Algorithm for Multidimensional Harmonic Retrivial, Ph.D. Thesis, Electrical Engineering and Information Sciences, Ruhr-Universität Bochum, Bochum, Germany, 2005.

[2] D. Nion, N.D. Sidiropoulos, Tensor algebra and multidimensional harmonic retrieval in signal processing for MIMO radar, IEEE Transactions on Signal Processing 58 (11) (2010) 5693–5705.

[3] M. Haardt, C. Brunner, J.H. Nossek, Efficient high-resolution 3-D channel sounding, in: Proceedings of the 48th IEEE Vehicular Technology Conference, Ottawa, ON, Canada, May 1998, pp. 164–168.

[4] K.N. Mokios, N.D. Sidiropoulos, M. Pesavento, C.E. Mecklenbrauker, On 3-D harmonic retrieval for wireless channel sounding, in: Proceedings of the IEEE International Conference on Acoustics, Speech Signal Process. (ICASSP'2004), vol. 2, May 2004, pp. 89–92.

[5] M. Haardt, R.S. Thomä, A. Richter, Multidimensional high-resolution parameter estimation with applications to channel sounding, in: Y. Hua, A. Gershman, Q. Chen (Eds.), High-Resolution and Robust Signal Processing, Marcel Dekker, New York, NY, 2004, pp. 255–338. Chapter 5.

[6] A. Bax, L. Lerner, Two-dimensional NMR spectroscopy, American Association for the Advancement of Science 232 (May) (1986) 960–967.

[7] Y. Li, J. Razavilar, K.J.R. Liu, A high-resolution technique for multi-dimensional NMR spectroscopy, IEEE Transactions on Biomedical Engineering 45 (January) (1998) 78–86.

[8] M.D. Zoltowski, C.P. Mathews, Real-time frequency and 2-D angle estimation with sub-Nyquist temporal sampling, IEEE Transactions on Signal Processing 42 (October) (1994) 2781–2794.

[9] D. Starer, A. Nehorai, Passive localization of near-field sources by path following, IEEE Transactions on Signal Processing 42 (March) (1994) 677–680.

[10] M. Haardt, J.A. Nossek, 3D unitary ESPRIT for joint 2-D angle and carrier estimation, in: Proceedings of the International Conference on Acoustics, Speech, and Signal Processing (ICASSP'1997), April 1997, vol. 1, pp. 255–258.

[11] P. Strobach, Total least squares phased averaging and 3D ESPRIT for join azimuth-elevation-carrier estimation, IEEE Transactions on Signal Processing 49 (January (1)) (2001) 54–62.

[12] X. Liu, N.D. Sidiropoulos, A. Swami, Blind high-resolution localization and tracking of multiple frequency hopped signals, IEEE Transactions on Signal Processing 50 (4) (2002) 889–901.

[13] M.D. Zoltowski, M. Haardt, C.P. Mathews, Closed-form 2-D angle estimation with rectangular arrays in element space or beamspace via unitary ESPRIT, IEEE Transactions on Signal Processing 44 (February) (1996) 316–328.

[14] M. Haardt, J.A. Nossek, Simultaneous Schur decomposition of several non-symmetric matrices to achieve automatic pairing in multidimensional harmonic retrieval problems, IEEE Transactions on Signal Processing 46 (January (1)) (1998) 161–169.

[15] M. Haardt, F. Roemer, G. Del Galdo, Higher-order SVD based subspace estimation to improve the parameter estimation accuracy in multi-dimensional harmonic retrieval problems, IEEE Transactions on Signal Processing 56 (July (7)) (2008) 3198–3213.

[16] A. Thakre, M. Haardt, K. Giridhar, Single snapshot R-D unitary tensor-ESPRIT using an augmentation of the tensor order, in: Proceedings of the IEEE International Workshop on Computational

Advances in Multi-Sensor Adaptive Processing, Aruba, Dutch Antilles, December 2009, pp. 81–84.
[17] H.L. Van Trees, Optimum Array Processing: Detection, Estimation, and Modulation Theory, Wiley, New York, 2002 Part IV.
[18] J. Liu, X. Liu, An eigenvector-based approach for multidimensional frequency estimation with improved identifiability, IEEE Transactions on Signal Processing 54 (December (12)) (2006) 4543–4556.
[19] M. Pesavento, C.F. Mecklenbräuker, J.F. Böhme, Multidimensional rank reduction estimator for parametric MIMO channel models, EURASIP Journal of Applied Signal Processing (September) (2004) 1354–1363.
[20] F.K.W. Chan, H.C. So, W. Sun, Subspace approach for two-dimensional parameter estimation of multiple damped sinusoids, Signal Processing 92 (September (9)) (2012) 2172–2179.
[21] W. Sun, H.C. So, Accurate and computationally efficient tensor-based subspace approach for multi-dimensional harmonic retrieval, IEEE Transactions on Signal Processing 60 (October (10)) (2012) 5077–5088.
[22] J.P.C.L. da Costa, F. Roemer, M. Haardt, R.T. de Sousa Jr., Multi-dimensional model order selection, EURASIP Journal of Advanced Signal Processing 2011 (26) (2011).
[23] K. Liu, H.C. So, L. Huang, A multi-dimensional model order selection criterion with improved identifiability, in: Proceedings of the International Conference on Acoustics, Speech, and Signal Processing (ICASSP 2012), Kyoto, Japan, March 2012, pp. 2441–2444.
[24] J. Rissanen, Modeling by shortest data description, Automatica 14 (1979) 465–471.
[25] H. Akaike, A new look at the statistical model identification, IEEE Transactions on Automatic Control 19 (6) (1974) 716–723.
[26] A. Quinlan, J.-P. Barbot, P. Larzabal, M. Haardt, Model order selection for short data: an exponential fitting test (EFT), EURASIP Journal of Applied Signal Processing (2007) 54–64.
[27] S. Kritchman, B. Nadler, Determining the number of components in a factor model from limited noisy data, Chemometrics and Intelligent Laboratory Systems 94 (2008) 19–32.
[28] S. Kritchman, B. Nadler, Non-parametric detection of the number of signals: hypothesis testing and random matrix theory, IEEE Transactions on Signal Processing 57 (10) (2009) 3930–3941.
[29] X.-D. Zhang, Y.-D. Li, Harmonic retrieval in mixed Gaussian and non-Gaussian ARMA noises, IEEE Transactions on Signal Processing 42 (12) (1994) 3539–3543.
[30] X.-D. Zhang, Y.-C. Liang, Y.-D. Li, A hybrid approach to harmonic retrieval in non-Gaussian ARMA noise, IEEE Transactions on Information Theory 40 (4) (1994) 1220–1226.
[31] B.M. Sadler, G.B. Giannakis, S. Shamsunder, Noise subspace techniques in non-Gaussian noise using cumulants, IEEE Transactions on Aerospace and Electron Systems 31 (3) (1995) 1009–1018.
[32] Y. Zhang, S. Wang, Harmonic retrieval in colored non-Gaussian noise using cumulants, IEEE Transactions on Signal Processing 48 (4) (2000) 982–987.
[33] R. Badeau, B. David, G. Richard, Selecting the modeling order for the ESPRIT high resolution method: an alternative approach, in: Proceedings of the IEEE International Conference on Acoustics, Speech and Signal Processing (ICASSP'2004), Montreal, Canada, May 2004.
[34] J.-M. Papy, L. de Lathauwer, S. van Huffel, A shift invariance based order-selection technique for exponential data modeling, IEEE Signal Processing Letters 14 (July) (2007) 473–476.
[35] J.P.C.L. da Costa, F. Roemer, D. Schulz, R.T. de Sousa, Subspace based multi-dimensional model order selection in colored noise scenarios, in: Proceedings of the IEEE Information Theory Workshop (ITW), October 2011, pp. 380–384.
[36] L. de Lathauwer, B. de Moor, J. Vanderwalle, A multilinear singular value decomposition, SIAM Journal on Matrix Analysis and Applications 21 (4) (2000) 1253–1278.
[37] F. Roemer, M. Haardt, Using 3-D unitary ESPRIT on a hexagonal shaped ESPAR antenna for 1-D and 2-D direction of arrival estimation, in: Proceedings of the International ITG/IEEE Workshop on Smart Antennas (WSA'05), Duisburg, Germany, April 2005.
[38] R.S. Thoma, M. Landmann, G. Sommerkorn, A. Richter, Multidimensional high-resolution channel sounding in mobile radio, in: Proceedings of the 21st IEEE Instrumentation and Measurement Technology Conference IMTC 04, vol. 1, 2004, pp. 257–262.
[39] H.M. Huizenga, J.C. de Munck, L.J. Waldorp, R.P.P.P. Grasman, Spatiotemporal EEG/MEG source analysis based on a parametric noise covariance model, IEEE Transactions on Biomedical Engineering 49 (June (6)) (2002) 533–539.
[40] B. Park, T.F. Wong, Training sequence optimization in MIMO systems with colored noise, in: Military Communications Conference (MILCOM 2003), Gainesville, USA, October 2003.